Journal of Nuclear Materials 401 (2010) 130–137

Contents lists available at ScienceDirect

Journal of Nuclear Materials

journal homepage: www.elsevier.com/locate/jnucmat

Analyses of dust samples collected in the MAST tokamak

C. Arnas [a,*], C. Pardanaud [a], C. Martin [a], P. Roubin [a], G. De Temmerman [b,1], G. Counsell [b,2]

[a] Laboratoire de Physique des Interactions Ioniques et Moléculaires, UMR 6633 CNRS-Université de Provence, 13397 Marseille, France
[b] EURATOM/CCFE Fusion Association, Culham Science Centre, OX14 3DB Abingdon, Oxfordshire, United Kingdom

ARTICLE INFO

Article history:
Received 11 February 2010
Accepted 9 April 2010

ABSTRACT

Dust samples collected in the MAST tokamak have been characterized. Mass measurements have been correlated to regions of collection. Electron microscopy has revealed the presence of large quantities of carbon nanoparticles produced in gas phase as well as the presence of rolled-up carbon thin layers whatever the collection region. Shape, structure and chemical composition have been established by means of complementary diagnostics such as electron microscopy, electron diffraction, energy dispersed X-ray spectroscopy, micro-Raman spectroscopy and infrared absorption spectroscopy.

1. Introduction

Erosion of plasma-facing materials by plasma–surface interaction is one of the primary processes that can lead to the production of fine particulate material or dust, in fusion devices [1–5]. A large amount of dust is expected to be produced in *ITER* and the consequent impact on safety and operational performance is the subject of ongoing study [6–8]. For example: dust on ITER surfaces at high temperature interacting with water steam released during a loss of coolant event could result in a potentially explosive hydrogen–oxygen mix, in the vacuum vessel; transport of dust outside the vacuum vessel could lead to contamination since the dust in ITER is likely to be toxic (i.e. containing Be) and radioactive (i.e. containing tritium and activated elements, mainly from W transmutation); the dust could affect the fuel inventory inside the ITER vacuum vessel, due to its large surface area and chemical reactivity which both lead to a propensity to retain deuterium/tritium; and lastly, because of the weak adherence of dust to surfaces, dust particles could be ejected into the ITER plasma, increasing the plasma contamination and potentially leading to plasma detachment and disruptions events [5,9,10].

Collection and analyses of dust in present day tokamaks can in principle help to improve understanding of dust formation and dust transport mechanisms, thereby improving the basis for extrapolating the likely dust quantities and location in ITER. Each device of course presents a unique design which has a profound impact on produced dust quantities and their distribution in existing devices and complicates extrapolation to ITER. On the other hand, when the plasma-facing components (PFCs) are carbon-based (as will be the case for some of the key ITER components during its early operational phase), similar dust morphology is observed, suggesting similar generation mechanisms [2,11].

In this paper we present analyses of dust samples collected from below the mid-plane of the MAST tokamak. Mass measurements have allowed us to identify regions of large dust deposition such as the plasma-shadowed areas [12,13]. Qualitative investigations have provided information on the shape, structure and composition. As usual in tokamaks with PFCs in graphite and stainless-steel vessel, we have observed by means of electron microscopy, the presence of micrometer irregular grains due to deposit flaking, micrometer smoothed grains which have undergone strong plasma erosion and particulates. In this latter case, we include both large quantities of carbon nanoparticles, gathered in agglomerates of several micrometers or in irregular layers which appear in all the samples and metallic particulates of size varying from the nanometer to the micrometer range. It is usually said that the former are synthesised in the plasma from the chemical and physical erosion of the PFCs and the later from arcing on vessel [2,5]. We have also found the presence of rolled-up thin carbon layers of several micrometer lengths which in our knowledge, were never observed in other tokamaks.

We have completed these investigations by Raman micro-spectroscopy, routinely used to characterize the different structure of C-based materials and have crossed the results with those found by high resolution transmission electron microscopy (HRTEM) and by electron diffraction. Infrared (IR) absorption spectroscopy has shown that carbon in the dust can be chemically bonded to other elements such as deuterium, hydrogen and for a small part, to oxygen.

* Corresponding author. Address: Laboratoire PIIM, UMR 6633 CNRS-Université de Provence, Faculté des Sciences de St Jerome, Case 321, 13397 Marseille, France. Tel.: +33 491288318.
E-mail address: cecile.arnas@univ-provence.fr (C. Arnas).
[1] Present address: FOM Institute for Plasma Physics Rijnhuizen, Edisonbaan 14, 3439 MN Nieuwegein, The Netherlands.
[2] Present address: Fusion for Energy, Josep Pla 2, Torres Diagonal Litoral B3, 08019 Barcelona, Spain.

0022-3115/$ - see front matter © 2010 Elsevier B.V. All rights reserved.
doi:10.1016/j.jnucmat.2010.04.010

The whole results are discussed. The measured quantities are correlated to the collection regions and we conclude on the carbon dust structure. Similarities and differences between the carbon nanoparticles synthesized in large quantities in the MAST tokamak and in laboratory plasmas are presented.

2. Dust collection

Dust was collected during a maintenance phase after the M6 operational campaign (2006-2007) of 4000 shots of ~0.3 s duration in average. After venting of the vacuum vessel and an initial safety control, dust collection was the first activity conducted inside the device, to minimise contamination or dust disturbance. The main method for sampling was the filtered vacuum technique used in other tokamaks [1–5]. For this, a stainless-steel filter housing was connected to a small oil-free vacuum pump. Two kinds of filters of 4.7 cm in diameter were used. Cellulose acetate filters which have the property to trap fine dust were chosen for dust mass measurement. They were weighted before and after collection. Cyclopore membranes characterized by controlled pore sizes (0.4 μm) were used for qualitative analyses by electron microscopy, IR absorption spectroscopy and Raman micro-spectroscopy.

Eight regions of collection by vacuuming have been selected below the mid-plane of the device (Fig. 1). These locations are divided in three groups: (i) erosion-dominated regions swept by plasma scrape-off layer (SOL) strike points, like the foot of the central column (inner divertor) and the outer divertor, made of 48 imbricated, radial tiles; (ii) the dome surface, which lies in the divertor private-flux region; and (iii) plasma-shadowed regions like the inner and outer toroidal grooves of the outer divertor tiles, the lateral ports and the upper surface of the poloidal magnetic coils which in MAST are the closest elements to the confined plasma on the outboard side [14].

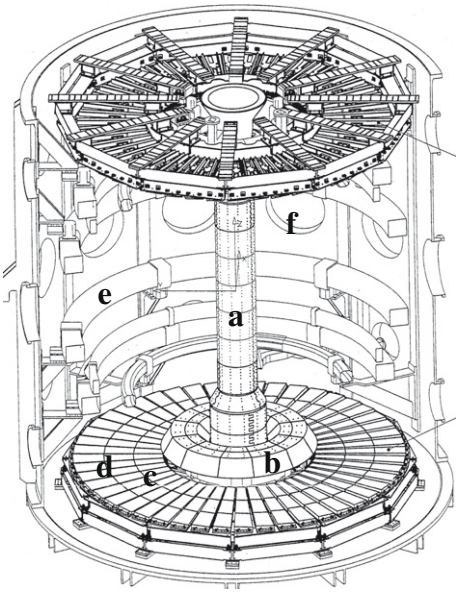

a: central column
b: dome
c and d: inner and outer toroidal grooves of the outer divertor tiles
e: magnetic coil
f: lateral port

Fig. 1. Scheme of the MAST tokamak.

The radial gap between the outer divertor tiles varies from 1.39 cm near the dome to 3.37 cm near the wall and significant quantity of dust is usually observed on the MAST vessel floor below these tiles. However, tile removal during this maintenance phase was not possible and dust from this area was not sampled.

The central column is made of polycrystalline graphite (EK986), the head and foot of the central column as well as the dome and the divertor tiles are made of polycrystalline graphite (EK98) while the vessel and the magnetic coil holders are in 304LN stainless-steel.

3. Mass measurement of mobilized dust

The largest quantity of dust was found in the outer toroidal groove of the divertor tiles (about 29.6 mg). For this estimation, dust was collected along the outer grove of three tiles and the corresponding mass was multiplied by 16. The same technique was applied for all the mass measurements.

By order of decreasing mass, we have found ~4.8 mg in the inner toroidal groove, about 4.2 mg in the lateral ports, ~4.1 mg on the dome surface and ~3.9 mg on the tile surface.

The total measured mass is ~46.6 mg but the total mass of dust produced during M6 campaign is certainly larger since no collection was performed on the vessel floor and on the upper half part of the device. However, the measurements performed in each of the three groups of MAST regions are consistent with dust transport studies in tokamaks. In particular, it is known that dust is transported towards the plasma-shadowed areas such as the gaps and grooves of divertor [12,13]. The largest quantity found in the outer toroidal grove is also consistent with the fact that the strike point in MAST sweeps the tile surface from the inner to the outer part without reaching the outer toroidal groove.

4. Dust morphology and composition

Scanning electron microscopy (SEM) analyses were performed directly on all the cyclopore filters with a PHILIPS XL30 SFEG microscope, using an electron beam of 10 kV. The microscope is coupled to an X-ray detector providing the composition by energy dispersed X-ray spectroscopy (EDX).

In the size range larger than 1 μm, SEM images show that dust particles are characterized by a wide range of size and shape as depicted in Fig. 2. As a general rule, whatever the investigated area, the dust contained four particle groups namely, carbonaceous grains of irregular shape, carbonaceous nanoparticles, metallic nano and microparticles and needles made of rolled-up thin carbon layers.

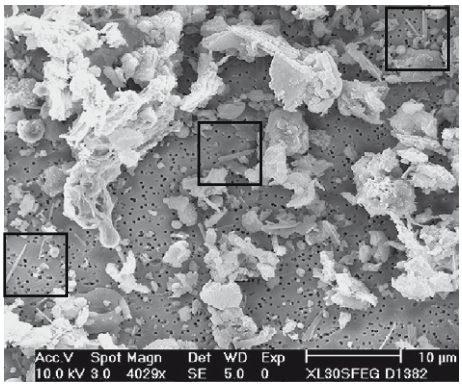

Fig. 2. SEM image showing dust of heterogeneous shape and size collected in the outer toroidal groove of the tiles (low magnification). Rolled-up thin carbon layers are shown into the three black squares.

At higher magnification, the SEM image in Fig. 3a shows surface details. There are two micrometer deposits of irregular shape, edge and roughness on the right and left side. At the image top, there is a spherical metallic microparticle of ~1.7 μm. EDX spectroscopy shows that these particulates usually contain C, Fe, Ni, Cr, O in different proportions. Some times, other elements such as Mo, Si and Ca are present. In the same image, carbon nanoparticles are gathered and form irregular layers below the black lines (Fig. 3a). Higher magnification of this image shows that these nanoparticles are so compressed under the black left line that it is difficult to individualize them whereas they are clearly identified in the black square whose magnification is given in Fig. 3b. They have size in the range of 15–30 nm.

Some carbonaceous grains exhibit smooth surfaces and edges as in Fig. 4 where a micrometer porosity is still visible. The whole aspect indicates a strong erosion. This grain is mixed with rolled-up thin carbon layers, observed in the majority of the dust samples. Examples are also shown in Fig. 2, in the three black squares. They can have several micrometer lengths and a width of ~1 μm or less.

Fig. 5a shows differences of texture between the grain of Fig. 4 and a dense agglomerate of nanoparticles (image bottom) whose magnification is given in Fig. 5b. Also here, one can see individual carbonaceous nanoparticles, providing a grain of large surface roughness in contrast with the grain of smoothed surface.

5. Dust morphology and structure analyses by TEM, HRTEM and electron diffraction

More details on dust morphology are provided by TEM. For this, we have transferred dust from all the acetate filters to thin polycarbonate films deposited on copper grids and investigated these samples with a JEOL JEM 2010F microscope operating with an electron beam of 200 kV. The highest magnification of this microscope allows having information on the atomic structure (HRTEM). The same beam was also used to perform electron diffraction.

HRTEM images have revealed that for a given sample, the carbonaceous flakes (thickness smaller than ~200 nm suitable for this diagnostic) present an heterogeneous organization at the atomic scale. The image can be that of amorphous carbon, i.e. without any order or that of disordered graphitic carbon, i.e. with fringes due to the stacking of graphene layers. For example, Fig. 6a and b shows images of flakes coming from the outer toroidal groove of tiles, characteristic of amorphous carbon whereas Fig. 6c and d shows that flakes can contain crumpled and folded graphite layers, oriented in different directions. In this later case, the flake was collected on the surface of the outer divertor tiles.

Fig. 7a provides another example of graphite made of graphitic crumpled layers and shells. The corresponding electron diffraction shows a Debye–Sherrer pattern containing Bragg 00*l* and *hk*0

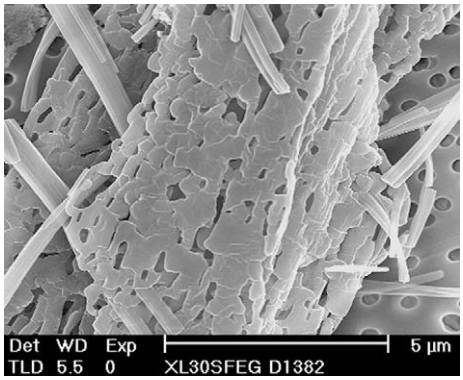

Fig. 4. SEM image of a smoothed surface grain and carbon rolled-up thin layers collected on the tile surface.

reflection (Fig. 7b). The 002 ring gives information on the stacking of graphitic layers parallel to the observation axis and the 100 and 110 rings, on that of oblique layers.

Fig. 7c gives an example of mixed material where metallic nanoparticles of 2–35 nm size produced from molten metal during arc discharges, are embedded in carbon deposits. The associated electron diffraction pattern (Fig. 7d) shows diffraction spots, attributed to electron diffraction on these metallic impurities. The diffraction rings corresponding to graphitic layers oriented in different directions are also present but are less intense than in Fig. 7b. Some of these metallic nanoparticles are polyhedral. They consist in a metallic core encapsulated in graphitic layers, parallel to the polyhedral sides. In Fig. 7e, the graphitic outer shell has ~6 nm width. All these features are characteristic of a catalytic growth process in gas phase where graphitisation occurs on melted metallic matter [15].

Carbonaceous spheroid nanoparticles are observed in all the dust samples. They also exhibit various structure. They can be amorphous as in Fig. 8a where the biggest have ~20 nm in size. In Fig. 8b, the sizes are similar but the particulates look like onion particles. They are made of concentric graphitic layers around amorphous cores.

6. Dust structure analyses by Raman spectroscopy

Raman micro-spectroscopy is routinely used to characterize different forms of C-based materials: diamond, graphite, disordered graphitic materials, amorphous carbons (a–C, a–C:H), etc. Interpreting the 1000–1800 cm^{-1} spectral region gives information on structural (degree of order) and chemical (hybridization of the carbon atoms) properties [16] and it was already used for characterizing carbon deposits in tokamaks [17,18].

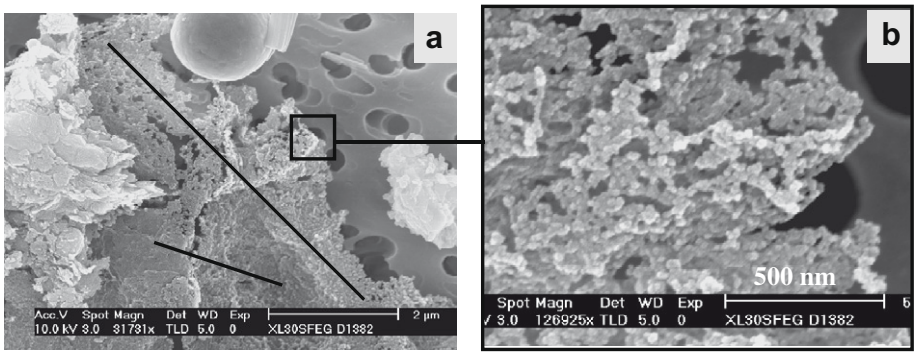

Fig. 3. (a) Dust collected on the dome surface and (b) magnification showing individual carbonaceous nanoparticles of 15–30 nm in size, gathered in an irregular layer.

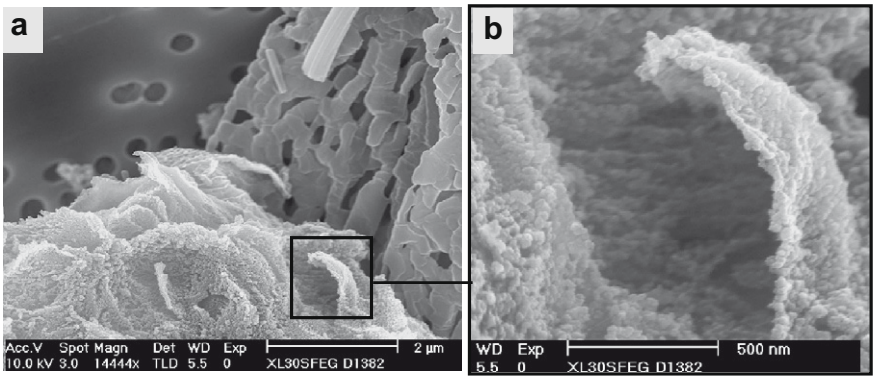

Fig. 5. (a) SEM image of two dust grains of different roughness at the bottom and right side and (b) magnification showing that the bottom grain is made of nanoparticles.

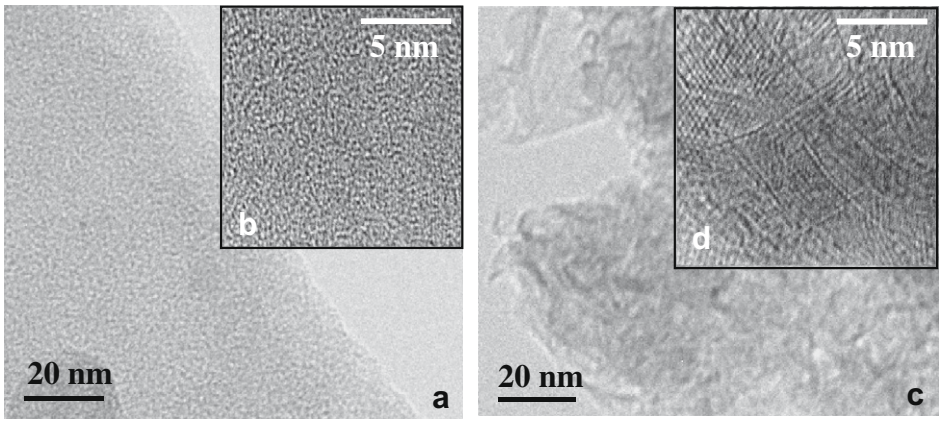

Fig. 6. TEM images of two flakes coming from the outer toroidal groove of tiles in: (a) and from the surface of the outer divertor tiles in (c). HRTEM shows amorphous carbon in (b) and graphitic layers in (d).

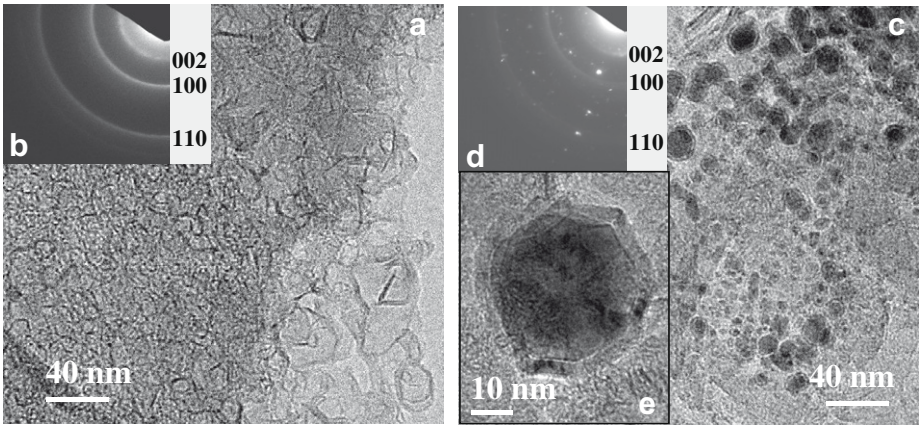

Fig. 7. (a) Disordered graphitic layers containing hollow shells, (b) corresponding diffraction pattern, (c) mixed material where metallic nanoparticles are embedded in carbon deposits, (d) corresponding diffraction pattern, (e) metallic nanoparticle encapsulated in graphitic layers.

Raman spectra were obtained using a Horiba-Jobin–Yvon HR LabRAM apparatus (laser wavelength: $\lambda_L = 514.5$ nm, 100X objective, resolution $\sim 1\ cm^{-1}$). Spectra were taken on grains as-collected, i.e. agglomerated on the cyclopore filters, and the thickest regions were probed to have enough matter. Several Raman spectra were recorded from all the regions where samples were collected. The laser power was chosen at $P \sim 2$ or ~ 0.2 mW μm^{-2} to have a good signal/noise ratio or to prevent damage. To check repeatability, spectra were recorded several times at the same spot and, in some cases, even at low power, a decrease of the background down to a constant value was observed. This indicates that molecular species, either in the sample composition or due to pollution, are burnt under laser irradiation. A linear background was then removed.

Fig. 9 displays the different kinds of spectra recorded for the dust samples, whatever the collection region, together with the spectrum of the virgin material EK98. Spectrum (a) is very close to this latter spectrum, most probably due to EK98 directly ablated from the wall. Spectra (b–d) are composed of two main bands at

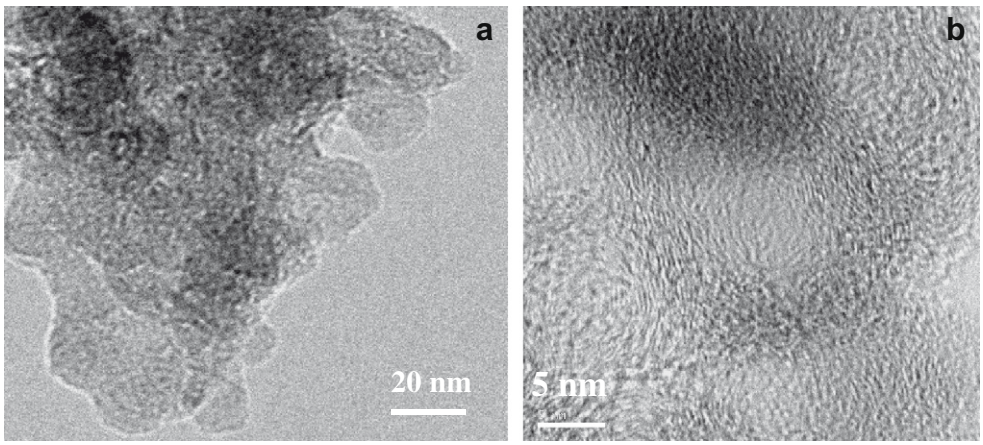

Fig. 8. (a) Nanoparticles of 20 nm mean size of amorphous carbon and (b) nanoparticles of similar size made of graphitic concentric layers, surrounding the amorphous carbon core.

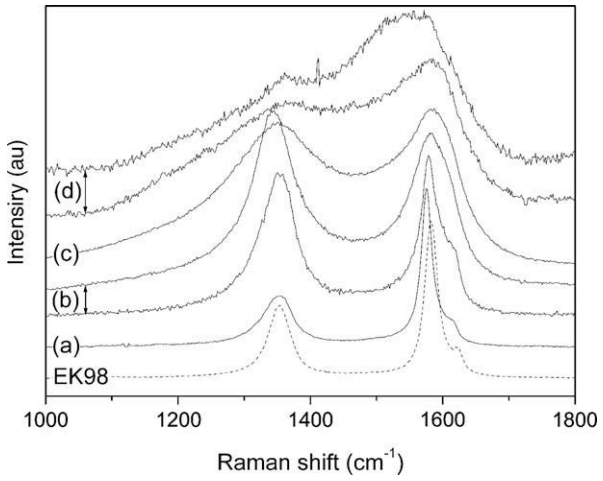

Fig. 9. Raman spectra from the different collection locations in MAST together with that of virgin EK98 (λ_L = 514.5 nm).

1570–1600 cm^{-1} (called the G band) and at ≈ 1350 cm^{-1} (called the D band). A third band sometimes appears as a shoulder of the former at 1620 cm^{-1} (called the D' band). These bands are assigned to stretching modes of sp^2 hybridized carbon atoms and are a signature of aromaticity, the aromatic domain size being limited by disorder [16,19].

When the D and G bands are well-separated, they correspond to graphitic carbon, even though disordered such as in the spectra (a–b) of Fig. 9, whereas when the two bands are broad and overlapped, they correspond to amorphous carbon such as in the spectra (d) [20]. Spectrum (c) is intermediate [21] and may correspond to heat treated amorphous carbon [20].

In the case of graphitic carbons, the D and G band relative intensity ratio noted R, varies, $R \approx 1$ being frequently observed everywhere in the machine. The Tuinstra relation, commonly used to estimate the length of the aromatic domains: L_a (nm) ≈ 4.4/R, leads here to L_a between 4 and 25 nm, the largest values being obtained for the best ordered material, such as EK98, and the smallest values being even larger than those of amorphous carbon (<2 nm). The great variety of Raman spectra indicates that dust structure is very heterogeneous. Nevertheless, dust collected on the divertor dome surface corresponds to the less ordered Raman signatures: no type-(a) spectra was recorded and type-(d) spectra were found only in this region. However, we cannot exclude the presence of other structures since the number of recorded spectra was not so large and since HRTEM also showed various structure in this region.

7. Infrared spectroscopy

Infrared absorption spectroscopy can be used to obtain relevant information on the chemical bonds and structure of carbonaceous material. The samples collected on the different locations of the device were all analysed by the Attenuated Total Reflectance unit (ATR) of a Bruker Vertex 70 FTIR infrared spectrometer, equipped with a germanium crystal (1.5 mm^2) and a DTGS detector. The spectra were recorded with 1000 scans and a resolution of 2 cm^{-1} from 3600 to 1000 cm^{-1}. For all samples, dust was extracted from the cyclopore membranes and set on the Ge crystal. Only the sample collected on the outer toroidal groove of tiles provided results with an adequate signal/noise ratio likely because enough material was found in this sample. A typical spectrum is displayed in Fig. 10.

The 3500–2400 cm^{-1} region (Fig. 10) is characterized by three bands. One of these bands is composed of two intense peaks at 2850 and 2920 cm^{-1} assigned respectively to the —CH_2 stretching symmetric and asymmetric modes of aliphatic compounds. Another intense band at 3293 cm^{-1} is assigned to the ≡CH stretching mode of monosubsituted acetylenic compounds. The small broad

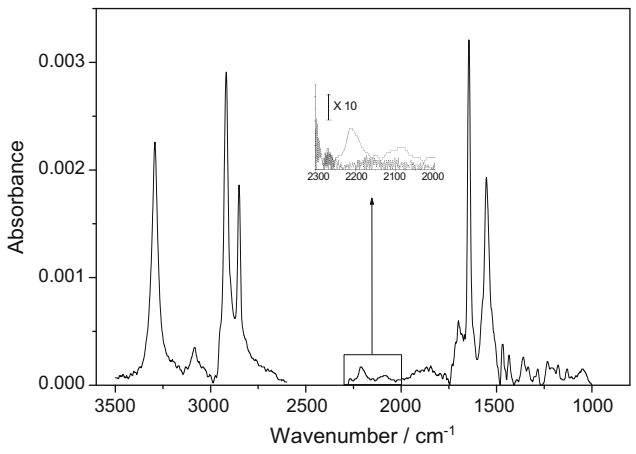

Fig. 10. Infrared absorbance spectrum of dust collected in the outer toroidal groove of the tiles. The inlet figure shows the CD stretching mode region, dust signal being compared to EK98 signal (lower curve).

band at 3100 cm^{-1} is assigned to the =CH stretching mode of polycyclic aromatic hydrocarbons and/or to the $=CH_2$ stretching mode of ethylenic compounds.

In 2400–1000 cm^{-1} region, a broad band at 1550 cm^{-1} and a narrow one at 1646 cm^{-1} are assigned respectively to the C=C stretching mode of polycyclic aromatic hydrocarbons and of ethylenic compounds. Small bands due to the $-CH_3$ and $-CH_2$ deformation modes are observed at 1470 and 1360 cm^{-1} respectively. Note that the low absorption signal at 1700 cm^{-1} is assigned to the C=O stretching mode, indicating that oxidation under air exposure is limited.

Samples collected in the outer toroidal groove of tiles then contain aromatic, ethylenic, and aliphatic signatures and are therefore probably highly heterogeneous.

The inlet of Fig. 10 emphasises the $=CD_2$ stretching mode of ethylene compounds at 2214 cm^{-1} and the small band at 2085 cm^{-1} which is assigned to the $-CD_2$ mode of poly(methylene) and/or to the C≡C stretching mode of alkyne compounds.

8. Discussion

Different complementary diagnostics have been used to characterize all the dust samples coming from the lower half part of MAST device. The collection regions have been divided into three groups: (i) erosion-dominated regions swept by strike points, (ii) divertor dome surface and (iii) plasma-shadowed regions.

Mass measurements have shown that the dust was preferentially collected in the plasma-shadowed regions, such as the lateral port and the tile grooves of the outer divertor. This result is consistent with specific studies which have shown that dust accumulation and fuel retention tend to occur in the gaps of castellated structures often found in tokamak plasma-facing components, including JET [12,22], TEXTOR [23] and TS [24]. In the previous design of MAST, measurements of deuterium density were performed by NRA on thin layers deposited on the shadowed area of ribs used as lower divertor [25]. The infrared absorption spectroscopy used in the studies reported here has allowed a qualitative investigation of the deuterium retention. In particular, we have found in the dust of the outer groove of the tiles the presence of deuterium through CD bond, indicating that deuterium is incorporated through chemical bonding during plasma operation.

By means of electron microscopy, we have found the same dust morphology in all the above-cited three regions. Grains of irregular shapes and edges coming from the flaking of deposited layers are easily identifiable by SEM, as for the other tokamaks [1–5]. By contrast, we have also observed grains of smoothed surfaces and edges which have undergone strong erosion, likely under ion bombardment.

HRTEM has revealed that the carbon structure of flakes is heterogeneous, varying from amorphous carbon to graphitic carbon. This latter structure corresponds to disordered graphitic carbon and is characterized here by the observation of graphene layer stacking of various thicknesses and lengths, oriented in various directions, sometimes forming shells. This structure was also quantified by micro-Raman spectroscopy which allows estimating the length of the aromatic domains, here from 4 to 25 nm. We have recorded spectra characteristic of disordered graphitic carbon in each dust sample except in that of the dome surface where we have observed the most disordered structure (amorphous carbon) even though we cannot exclude the presence of other structures seen by HRTEM. Everywhere else, we have also obtained spectra comparable to the reference spectrum of the EK98 graphite of MAST PFCs. This latter result suggests that grains may be released from the PFCs during transient events and without significant interaction with the plasma, whose effect would be to induce disorder and to destroy the graphitic structure.

IR absorption spectra have confirmed that dust collected in the outer toroidal groove of tiles has a carbon heterogeneous structure. Besides the graphitic carbon identified through the =CH and C=C stretching modes assigned to aromatic domains, we have also found the presence of polymer like carbon through =CH ethylenic groups and CH aliphatic groups which participate to the amorphous carbon structure. Other dust samples have provided essentially flat spectra, likely because there was not enough material for the analyses.

The flakes can contain metallic impurities most often under the shape of spherical nanoparticles, produced in gas phase. Metallic nanoparticles encapsulated into graphite layers are also generated through catalytic effect. When the sizes are in the micrometer range, microparticles are rather dispersed onto the dust samples, among other kind of dust. It is usually said that these metallic nano and microparticles are produced from arcing discharges [26] which take place on the device vessel as well as here, on the magnetic coil holders where their traces are observed. Indeed, laboratory arc discharges are routinely used to generate metallic powders following the way: (i) evaporation of a metallic cathode by hot arc plasma jets and (ii) cooling/condensation of the released vapour in thermal gradient which are produced between the electrode source and the water-cooled walls of the chamber [27] or in an inert gas flow [28].

In the MAST tokamak, we have also observed the presence of rolled-up carbon layers, not identified in other tokamaks. HRTEM has shown that they are graphitic and can be very thin (less than 100 nm). Their flaking and rolling-up could be due to a thermal expansion coefficient different from that of the substrate [29].

Whatever the collection region, the analyses have shown the presence of large quantities of carbonaceous nanoparticles produced in gas phase. SEM images show that they are gathered to form irregular agglomerates and layers of several micrometers. The biggest size measured by SEM was about 40 nm and the lowest by HRTEM was about 3 nm. Nanoparticles of these typical sizes cannot be detected by optical microscopy or even by SEM, operating in the micrometer range magnification which were typically used to establish size distribution in previous dust analysis campaigns [1,3]. Recently, size distribution and average dust density measurements were established as a function of location in the scrape-off layer region in DIII-D tokamak by scattering of a Nd: Yag laser [30]. But in a first calculation using Rayleigh approximation, the minimum size was estimated to be 55 nm and then 160 nm, using Mie-scattering model and taking into account dust ablation by the laser [31]. Optical imaging with cameras during tokamak operation revealed only the presence of individual big dust particles [32,33]. However, in previous dust analyses, TEM revealed the presence of nanoparticles of ~15 nm diameter in Tore Supra [4] and more recent analyses by HRTEM showed, still in this tokamak the presence of onion-like nanoparticles of size as low as 5 nm [17,34]. Therefore, the use of electron microscopy over different scale lengths is confirmed as an essential diagnostic to detect nanoparticles produced in gas phase, that cannot be observed by in situ diagnostics.

It is now admitted that nanoparticles can grow in divertor and SOL plasmas from hydrocarbon molecules released during the PFCs chemical erosion and from sputtered carbon atoms during the PFCs physical erosion [2,35]. Roughly speaking, there are two stages leading to particulate synthesis in cold plasmas. The first one concerns the growth of neutral and ionic molecular precursors through chemical reactions which are still not well identified. The second one concerns the growth of solid particles in the plasma when nucleation has occurred.

Carbon nanoparticles have already been produced from laboratory discharges in low pressure hydrocarbon gases such those

released by the graphite PFCs: in methane [36,37], ethylene [36], acetylene [36,38], in methane/ethylene mixture [39] and also at higher pressure, for instance in $Ar/CH_4/H_2$ mixture [40]. These experiments have pointed out that the chemical reactions which lead to nucleation depend strongly on discharges and plasma conditions. Modeling even shows that discharges in the same hydrocarbon gas lead to different complex chemical pathways and therefore to different molecular precursors if discharge parameters are different [41,42]. In tokamaks, difficulties are amplified by the fact that chemical and physical erosion of graphite PFCs may occur at the same time, adding carbon clusters to the gas mixture near the wall which also lead to nucleation by condensation [43] and/or by cluster reactions, involving clusters with magic numbers [44].

It is worth noting that in laboratory plasmas of low pressure, whatever the nature of the molecular precursors and the operation mode, the dust deposits on substrates are similar to those of Figs. 3b and 5b. They are made of dense nanoparticle agglomerates, where nanoparticles in the same size range are visible i.e. they are not embedded in deposited layers. This is one of the features of dusty plasmas where clouds of nanoparticles at high concentration are generated and where, after nucleation, the molecular precursors participate to the dust growth through their sticking on dust surface instead of creating new nuclei [45], this fact explaining the uniform sizes. Moreover, nanoparticles of onion-like texture as in Fig. 8b are observed in a wide range of carbonaceous nanoparticle production: from sputtering discharges, arc discharges to hydrocarbon discharges. This fact clearly shows that the final carbon texture cannot give information on the molecular precursors but indicates at least that nanoparticles were synthesized and transported in a hot medium [46] or were heated by high particle fluxes [47,48] since the graphitic ordering of the concentric texture is enhanced by rising temperature [49].

9. Conclusions

We have reported mass measurement and qualitative analyses of dust samples, vacuumed in the MAST tokamak, in three main regions located below the mid-plane of the device such as eroded-dominated regions swept by strike points, the divertor dome surface and plasma-shadowed regions. Mass measurements have provided a scale of dust deposition and show that they are mainly deposited in shadowed areas (grooves and lateral ports). By means of infrared absorption spectroscopy, deuterium was found on dust of the outer grove of the divertor tiles indicating that fuel co-deposition is of chemical nature and occurs during plasma operation. Elsewhere, essentially flat spectra were obtained likely because there was not enough matter for analyses. The SEM images have not revealed differences in the dust shape and nature as a function of the region. We have observed everywhere micrometer grains coming from the flaking of deposited layers. Among them, we have found flakes characterized by smoothed surfaces and edges, likely produced by strong plasma erosion. We have found large quantities of carbon nanoparticles produced in gas phase, gathered to form micrometer agglomerates and layers. Metallic nanoparticles were also observed, either embedded in carbonaceous deposit layers when they have nanometer sizes or dispersed into the dust samples when they have size in the micrometer range. We have found everywhere, rolled-up graphitic thin layers not observed in other tokamaks. HRTEM, electron diffraction, micro-Raman spectroscopy and IR absorption spectroscopy have shown that the structure of the carbon dust is highly heterogeneous. It varies from amorphous to graphitic carbon, the former structure being observed only on the dome surface by micro-Raman spectroscopy. In addition, grains similar to EK98 graphite of MAST PFCs have been found almost everywhere, probably directly extracted from the PFCs.

Acknowledgements

The authors would like to express their gratefulness to P. Sharpe, P. Chappuis and C. Brosset for their invaluable help and advices to collect dust and also to E. Delchambre, N. Fawlk and S. Booth for their appreciable help in the organization of dust collection in the MAST tokamak. The CCFE authors were funded by the UK EPSRC. This work made within the framework of EFDA and the French FR-FCM was supported by EURATOM/CEA association contract.

References

[1] W.J. Carmack, K.A. McCarthy, D.A. Petti, A.G. Kellman, C.P.C. Wong, Fusion Eng. Des. 39–40 (1998) 477.
[2] J. Winter, Plasma Phys. Controlled Fusion 40 (1998) 1201.
[3] A.T. Peacock, P. Andrew, P. Cetier, J.P. Coad, G. Federici, F.H. Hurd, M.A. Pick, C.H. Wu, J. Nucl. Mater. 266 (1999) 423.
[4] Ph. Chappuis, E. Tsitrone, M. Mayne, X. Armand, H. Linke, H. Bolt, D. Petti, J.P. Sharpe, J. Nucl. Mater. 290–291 (2001) 245.
[5] J.P. Sharpe, D.A. Petti, H.W. Bartels, Fusion Eng. Des. 63–64 (2002) 153.
[6] K.A. McCarthy, D.A. Petti, W.J. Carmack, G.R. Smolik, Fusion Eng. Des. 42 (1998) 45.
[7] G. Federici, C.H. Skinner, J.N. Brooks, J.P. Coad, C. Grisolia, A.A. Haasz, A. Hassanein, V. Philipps, C.S. Pitcher, J. Roth, W.R. Wampler, D.G. Whyte, Nucl. Fusion 41 (2001) 1967.
[8] J. Roth, E. Tsitrone, A. Loarte, Th. Loarer, G. Counsell, R. Neu, V. Philipps, S. Brezinsek, M. Lehnen, P. Coad, Ch. Grisolia, K. Schmid, K. Krieger, A. Kallenbach, B. Lipschultz, R. Doerner, R. Causey, V. Alimov, W. Shu, O. Ogorodnikova, A. Kirschner, G. Federici, A. Kukushkin, J. Nucl. Mater. 390–391 (2009) 1.
[9] D.H.J. Godall, J. Nucl. Mater. 111–112 (1982) 11.
[10] A. Ekedahl, J. Bucalossi, Y. Corre, E. Delchambre, G. Dunand, O. Meyer, R. Mitteau, P. Monier-Garbet, B. Pégourié, F.G. Rimini, F. Saint Laurent, J.L. Schwob, E. Tsitrone, J. Nucl. Mater. 390–391 (2009) 806.
[11] J.P. Sharpe, B.J. Merril, D.A. Petti, M.A. Bourham, J.G. Gilligan, J. Nucl. Mater. 290–291 (2001) 1128.
[12] J.P. Coad, M. Rubel, C.H. Wu, J. Nucl. Mater. 241–243 (1997) 408.
[13] M.J. Rubel, J.P. Coad, P. Wienhold, G. Matthews, V. Philipps, M. Stamp, T. Tanabe, Phys. Scr. 11 (2004) 112.
[14] W. Xiaomin, X. Bingshe, J. Husheng, L. Xuguang, I. Hideki, J. Phys. Chem. Solids 67 (2006) 871.
[15] A.C. Darke, R.J. Hayward, G.F. Counsell, K. Hawkins, Fusion Eng. Des. 75–79 (2005) 285.
[16] F. Tuinstra, J.L. Koenig, J. Chem. Phys. 53 (1970) 1126.
[17] M. Richou, C. Martin, P. Delhaès, M. Couzi, C. Brosset, B. Pégourié, A. Litnovsky, V. Phillips, P. Wienhold, J. Dentzer, C. Vix-Guterl, P. Roubin, Carbon 45 (2007) 2723.
[18] Y. Raitses, C.H. Skinner, F. Jiang, T.S. Duffy, J. Nucl. Mat. 375 (2008) 365.
[19] M.J. Matthews, M.A. Pimenta, G. Dresselhaus, M.S. Dresselhaus, M. Endo, Phys. Rev. B 59 (1999) 6585.
[20] A.C. Ferrari, J. Robertson, Philos. Trans. R. Soc. A 362 (2004) 2477.
[21] C. Pardanaud, C. Martin, P. Roubin, W. Jacob, T. Schwartz-Sellinger, Carbon'09, The Annual World Conference on Carbon, Topic 08, n°528, Biarritz, France.
[22] M.J. Rubel, J.P. Coad, R.A. Pitts, J. Nucl. Mater. 367–370 (2007) 1432.
[23] A. Litnovsky, V. Phillips, P. Wienhold, G. Sergienko, B. Emmoth, M. Rubel, U. Breuer, E. Wessel, J. Nucl. Mater. 337–339 (2005) 917.
[24] B. Pégourié, C. Brosset, E. Tsitrone, A. Beauté, S. Brémond, J. Bucalossi, S. Carpentier, Y. Corre, E. Delchambre, et al., J. Nucl. Mater. 390–391 (2009) 550.
[25] A. Tabasso, G.F. Counsell, D. Hole, J.P. Coad, J. Nucl. Mater. 306 (2002) 73.
[26] J. Winter, G. Gebauer, J. Nucl. Mater. 266–269 (1999) 228.
[27] J.P. Lei, X.L. Dong, X.G. Zhu, M.K. Lei, H. Huang, X.F. Zhang, B. Lu, W.J. Park, H.S. Chung, Intermetallic 15 (2007) 1589.
[28] C. Qin, S. Coulombe, Plasma Sources Sci. Technol. 16 (2007) 240.
[29] A. Reina, X. Jia, J. Ho, D. Nezich, H. Son, V. Bulovic, M.S. Dresselhaus, J. Kong, Nano Lett. 9 (2009) 30.
[30] W.P. West, B.D. Bray, J. Burkart, Plasma Phys. Controlled Fusion 48 (2006) 1661.
[31] R.D. Smirnov, W.P. West, S.I. Krasheninnikov, A. Yu Pigarov, M. Rosenberg, B.D. Bray, Phys. Plasmas 14 (2007) 112507.
[32] D.L. Rudakov, J.H. Yu, J.A. Boedo, E.M. Hollman, S.I. Krasheninnikov, et al., Rev. Sci. Instrum. 79 (2008) 10F3003.
[33] G. De Temmerman, Private Communication.
[34] P. Roubin, B. Pégourié, R. Smirnov, C. Martin, M. Richou, Y. Marandet, C. Pardanaud, C. Brosset, J. Gunn, J. Nucl. Mater. 390–391 (2009) 49.
[35] P. Sharpe, B.J. Merril, D.A. Petti, M.A. Bourham, J.G. Gilligan, J. Nucl. Mater. 290–293 (2001) 1128.
[36] Ch. Deschenaux, A. Affolter, Ch. Hollenstein, P. Fayet, J. Appl. Phys. 32 (1999) 1876.

[37] I. Géraud-Grenier, V. Massereau-Guilbaud, A. Plain, Surf. Coat. Technol. 187 (2004) 336.
[38] E. Kovacevic, L. Stefanovic, J. Berndt, J. Appl. Phys. 93 (2003) 2924.
[39] S. Hong, J. Berndt, J. Winter, Plasma Sources Sci. Technol. 12 (2003) 46.
[40] N. Aggadi, C. Arnas, F. Bénédic, C. Dominique, X. Duten, F. Silva, K. Hassouni, Diamond Relat. Mater. 15 (2006) 908.
[41] S. Stoykov, C. Eggs, U. Kortshagen, J. Phys. D: Appl. Phys. 34 (2001) 2160.
[42] K. Hassouni, F. Mohasseb, F. Bénédic, G. Lombardi, A. Gicquel, Pure Appl. Chem. 78 (2006) 1127.
[43] P.D. Haaland, A. Garscadden, B. Ganguly, S. Ibrani, J. Williams, Plasma Sources Sci. Technol. 3 (1994) 381.
[44] C. Arnas, A. Mouberi, K. Hassouni, A. Michau, G. Lombardi, X. Bonnin, F. Bénédic, B. Pégourié, J. Nucl. Mater. 390–391 (2009) 140.
[45] L. Boufendi, A. Plain, J.Ph. Blondeau, A. Bouchoule, C. Laure, M. Toogood, Appl. Phys. Let. 60 (1992) 169.
[46] C. Arnas, A. Mouberi, K. Hassouni, G. Lombardi, F. bénédic, X. Bonnin, AIP Conf. Proc. 1041 (2005) 33.
[47] R.D. Smirnov, A. Yu Pigarov, M. Rosenberg, S.I. Krasheninnikov, D.A. Mendis, Plasma Phys. Controlled Fusion 49 (2007) 347.
[48] C. Arnas, A. Mouberi, J. Appl. Phys. 105 (2009) 063301.
[49] J.N. Rouzaud, A. Oberlin, Carbon 27 (1989) 517.